https://doi.org/10.30898/1684-1719.2020.6.15
UDC 621.371; 621.372.832

A TUNABLE MULTIBAND MICROWAVE FILTER BASED ON A WAVEGUIDE TEE INTERFEROMETER CONTAINING FABRY–PEROT RESONATOR WITH A METASTRUCTURE AS A REFLECTOR

G. A. Kraftmakher, V. S. Butylkin, Yu. N. Kazantsev, V. P. Mal'tsev, I. P. Nikitin

Fryazino Branch of Kotelnikov Institute of Radioengineering and Electronics of Russian Academy of Sciences, Vvedensky Sq.1, Fryazino Moscow region 141190, Russia

The paper is received on June 15, 2020

Abstract. A new way to achieving selectively electrically tunable multiband microwave filtering is proposed that is based on a modified *h*-plane 3–6 GHz waveguide tee interferometer containing a tunable metastructure. The metastructure is placed along the wave propagation direction in the short-circuited *h*-arm at a distance from the short, thus forming the configuration of a Fabry–Perot resonator. Various functionalities of the interferometer are revealed and demonstrated through the use of various varactor-loaded metastructures such as a wire metastructure, a butterfly dipole, a row of split ring resonators, and a rings/dipole sandwich. The possibility of selective tuning of the band center frequency (by 0.2 GHz with a wire metastructure and a butterfly dipole), or a selective change in the shape and width of each stop-band by turns (with split ring resonators), or a change in the shape and width of each stop-band and center frequency independently (with a "split ring resonators--butterfly dipole" sandwich) is demonstrated. The tuning of the interference bands in the resonator and the interferometer is related to the effect of tunable resonance in the metastructure, which occurs when the resonance frequency in the metastructure approaches the appropriate interference band.

Keywords: filtering, selective electrical tuning, tee waveguide interferometer, metastructure, varactor, microwaves, Fabry-Perot resonator, interference bands tuning.

Introduction

Tunable multiband electromagnetic wave filters are in constant demand in multichannel communication systems; therefore, interest in new developments in this field persists over time [1]. These filters are based on a cascade of different-range resonators combined with a transmission line. Meta-atoms and, meta-surfaces based on conducting ring elements compatible with tuning elements and multilayer structures have been suggested as the resonators. Methods that have been approved in single-band filters are used to control and tune these filters. These methods are based on electromechanical [2, 3], magnetic (with the use of ferrites) [4–6], and electric (with the use of ferroelectric capacitors) [7] effects and on semiconductor varactors [8, 9]. Nonreciprocal resonant metastructures containing ferrite and conducting elements with varactors have been proposed as a basis for nonreciprocal filters compatible with the magnetic and electric methods of control. For example, in [10, 11], the authors investigated a "ferrite plate/row of magnetically excited varactor-loaded split rings" metastructure [10] and a nonreciprocal three-layer metastructure combined with a ferrite plate [11] in a rectangular waveguide in an external dc magnetic field. Fabry–Perot resonators have been extensively investigated as antenna elements. To tune these resonators, one usually changes the optical distance between the mirrors, using a moving mirror mounted on a piezoceramic drive, or filling the space between the mirrors with a medium and changing its permittivity by an external field. Recently, Fabry–Perot resonators have been considered in which Bragg gratings [12] or frequency-selective and meta-surfaces [13] are used as reflectors. However, the possibility of tuning of microwave Fabry–Perot resonators has hardly been investigated. To date, reconfigurable multiband filters involving a cascade of different-range resonators or devices have been successfully developed [14, 15, 16] that allow switching between frequency bands. Moreover, the authors of [17–20] used reconfiguration and smooth tuning within each design. In [17], the authors demonstrated an antenna that is both frequency tunable and polarization reconfigurable. The frequency tuning is achieved by tuning varactor diodes, while polarization is reconfigured by switching the feeding circuit of the antenna. In [18],

the authors used two pairs of half-wavelength resonators loaded with varactors to design a dual-band bandpass-to-bandstop filter with tunable center frequency of each band, in which PIN diodes were used to switch from the bandpass to the bandstop state of the filter. The paper [21] provides an overview of recent reconfigurable microwave filters and presents references to several types of tunable microstrip filters, especially those related to new design technologies. Recently, some publications have appeared that are devoted to the implementation of filters based on substrate integrated waveguide (SIW) technology, in which the height of a filter is much smaller than the height of a filter based on the classical rectangular waveguide and corresponds to the thickness of the dielectric substrate [22, 23]. The emphasis was placed on the miniaturization and the use of new materials, as well as on the tunability. The reported filters allow controlled one- or two- band filtering of microwaves. However, as pointed out in [24]**,** there are certain difficulties with tuning in the case of multiband (three or a greater number of bands) filtering.

Today, along with successfully developing controlled optical interferometry, microwave interferometers have been suggested to be used as tunable multiband filters [25, 26]. In [25], the authors investigated a Mach–Zehnder microwave interferometer based on a ferrite–ferroelectric layered structure. In [26], the authors used a metastructure as a beam splitter in a modified waveguide tee interferometer and demonstrated the possibility of magnetic and electric control of a multiband interferogram in the case when the metastructure consists of a ferrite plate and varactor-loaded dipoles or rings.

The present paper is devoted to the development of tunable multiband microwave filters using microwave interferometry. We propose a new way to achieve selective electrically tunable multiband microwave filtering that is implemented through the use of a 3–6 GHz *h*-plane modified waveguide tee-interferometer containing a tunable metastructure as a reflector in a Fabry–Perot resonator combined with the interferometer. The metastructure is placed along the wave propagation direction in the short-circuited *h*-arm at a distance from the short, thus forming the configuration of a reflection-type Fabry–Perot resonator. We have found that the

tuning of the interference bands in the resonator and the interferometer is related to a tunable resonance in the metastructure and occurs when the resonance frequency of the metastructure approaches the corresponding band. We demonstrate this effect and various interferometer functionalities by using different varactor-loaded metastructures. The first metastructure is an easy-to-fabricate two-layer metasructure in which the first layer represents a grating of parallel copper wire segments and the second layer is an orthogonal asymmetrically placed split narrow copper strip loaded with a varactor diode. Resonance effects in similar metastrucrures, as well in a magneticaly and electrically tunable nonreciprocal three-layer metastructure in which the third layer is a ferrite plate [11], were investigated in a rectangular waveguide and in free space [27]. The second metastructure is a butterfly dipole, and the third is a row of doubly split ring resonators. We also verify the observed effects with the use of similar metastructures without varactor loading, in which the effect of the varactor diode is achieved through the use of strips of different length or a dipole of different fixed capacitance.

In the present paper, we investigate for the first time a modified microwave waveguide interferometer based on an *h*-plane tee that contains a reflection-type Fabry–Perot resonator. One of reflectors of the resonator represents an electrically controlled metastructure. We demonstrate that the multifrequency spectrum of the resonator and interferometer can be tuned by an external action on the resonant properties of the metastructure, rather than by changing its length, as is usually done. We show that the proposed interferometer offers wide possibilities for designing various multiband filters and for selective electric control of their properties.

1. Interferometer

The interferometer (Fig. 1a) is based on an *h*-plane waveguide tee with a controlled metastructure.

The metastructure is situated in the *h*-arm *3* (the length of the *h*-arm is 290 mm) along the wave propagation direction at distance s_m =110 mm from the short and forms the configuration of a reflection-type Fabry–Perot resonator *4*. We use a single-channel measurement method and measure the transmission coefficient $T = S_{21}$

(which characterizes the insertion loss) of the interferometer, as well as the reflection coefficient $R = S_{11}$ (which characterizes the return loss), in a 48x24 mm rectangular waveguide (WG) in the frequency band 3–6 GHz by a panoramic VSWR meter. An empty rectangular waveguide *h*-plane tee (Port 1 is the input) is transformed into an interferometer and acts as a multiband filter provided that Port 3 is short-circuited (Fig. 1b). To increase the number of interference bands, one should increase the length of the short-circuited arm.

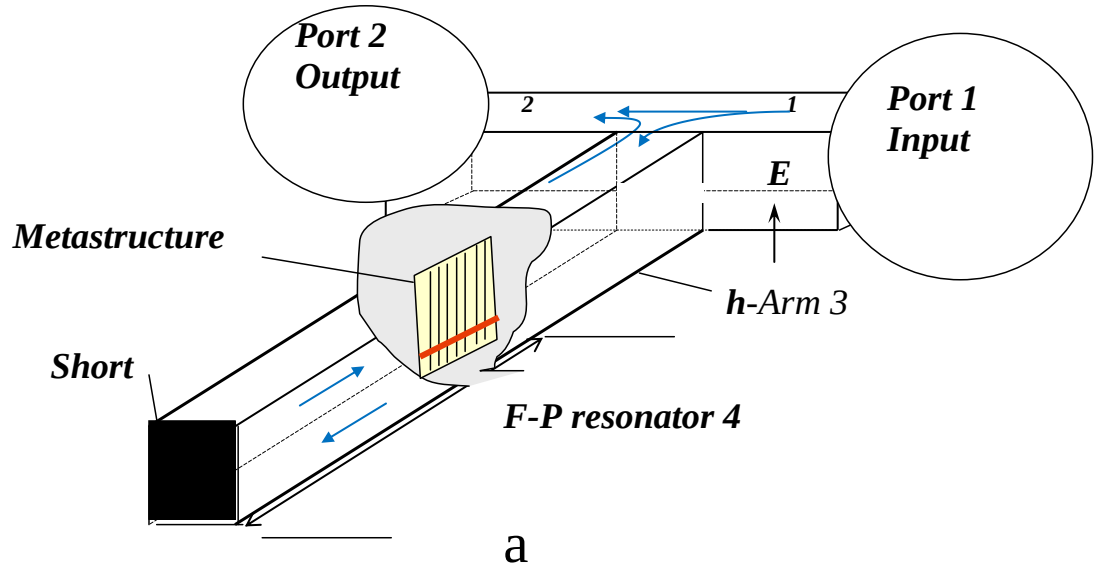

a

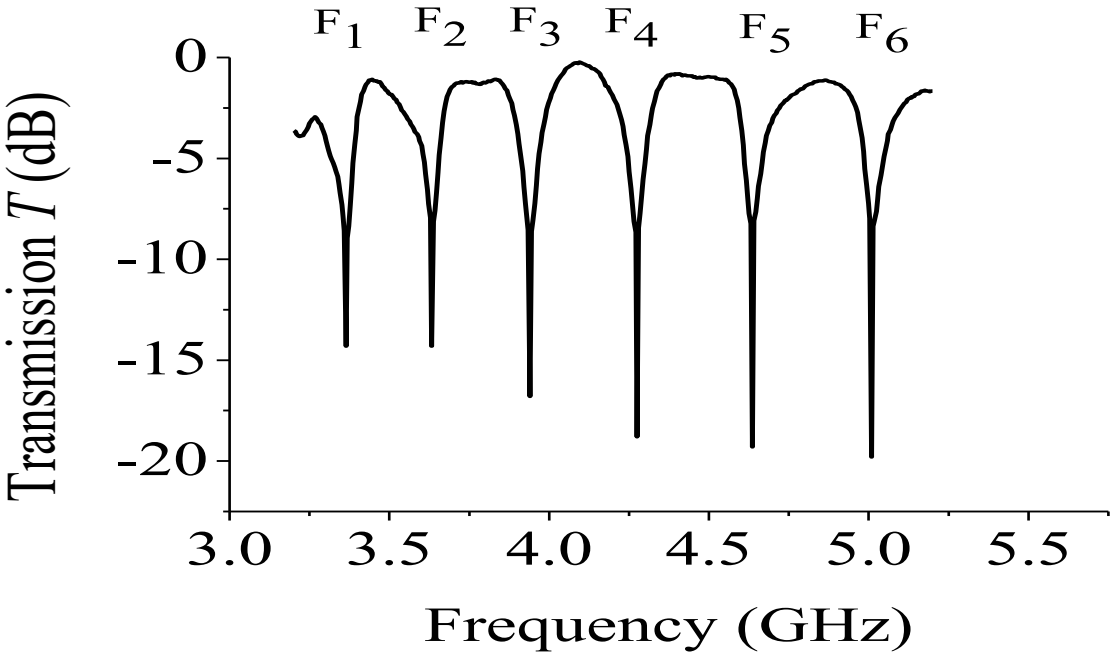

b

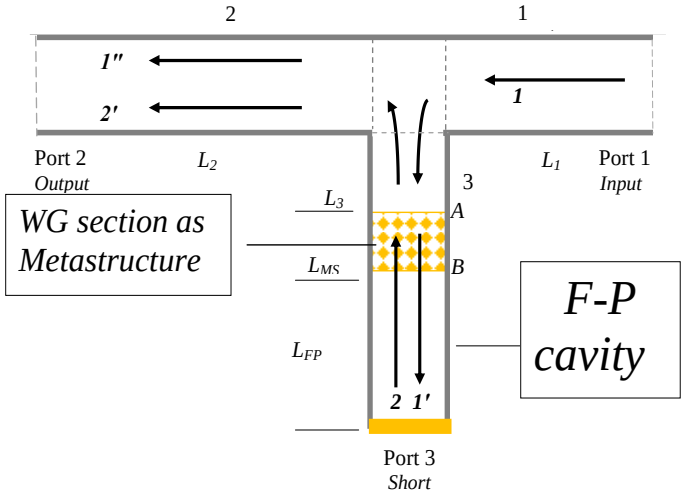

c

Fig. 1. Proposed tee interferometer. (a) Scheme, (b) Transmission without metastructure, (c) Scheme for description by s-matrix.

One can easily verify that such a device can be used to obtain controlled interferograms by introducing an ***s***-matrix with elements $s_{mn} = |s_{mn}|\exp(i\varphi_{mn})$ to describe signal transmission between the arms of the interferometer, as in [26]. We model a metastructure by a waveguide section filled with a controlled metamaterial (Fig. 1c). The arrows with triangular heads indicate the signal propagation directions.

The amplitude coefficient of signal transmission from the arm *1* to the arm *2*,

$$s = s_{21} + s_{23} r^{(FP)} s_{31} \exp\left(-2ik_3 L_3\right)\Big) \times\left[1 - r^{(FP)} s_{33} \exp\left(-2ik_3 L_3\right)\right]^{-1} \quad (1)$$

consists of the amplitude coefficient of direct transmission between these arms and the amplitude transmission coefficient of a signal that is tapped off from the input arm to arm *3* and then is also fed to the output arm.

This part of the signal experiences multiple reflections between the junction region of the arms of the interferometer and the Fabry–Perot resonator, which consists of the short, the metastructure, and the hollow waveguide section between them. The amplitude reflection coefficient from the Fabry–Perot resonator is obtained in [28] when deriving the Airy formulas and is given by

$$r^{(FP)} = r_{33}^{(MS)} + t_{C3}^{(MS)} r_{\text{short}} t_{3C}^{(MS)} \exp\left(-2ik_{FP}L_{FP}\right) \times\left[1 - r_{CC}^{(MS)} r_{\text{short}} \exp\left(-2ik_{FP}L_{FP}\right)\right]^{-1} \quad (2)$$

in our notations. The indices *1* and *2* refer to the input and output arms of the interferometer, the index *3*, to the input section of the arm that contains the Fabry–Perot resonator, and the index *C* refers to the cavity of the resonator. We also introduced the following notation: k_m is the propagation constant of the *m*-th arm, L_m is the path traveled by a wave in this arm, L_{FP} is the length of the waveguide in the Fabry–Perot resonator, k_{FP} is the propagation constant of this waveguide, and $r_{\text{short}} = |r_{\text{short}}|\exp(i\varphi_{\text{short}})$ is the amplitude reflection coefficient from the short of the interferometer. The quantities $r_{mn}^{(MS)} = \left|r_{mn}^{(MS)}\right|\exp\left(i\varphi_{mn}^{r}\right)$ and $t_{mn}^{(MS)} = \left|t_{mn}^{(MS)}\right|\exp\left(i\varphi_{mn}^{t}\right)$ are the amplitude reflection and transmission coefficients of the metastructure situated between the waveguide sections with indices *m* and *n*. Namely, $r_{33}^{(MS)}$ is the reflection coefficient of the metastructure for a signal coming from waveguide *3*, $r_{CC}^{(MS)}$ is the reflection coefficient of the metastructure for a signal coming from the short, and $t_{3C}^{(MS)}$ and $t_{C3}^{(MS)}$ are the transmission coefficients of the metastructure for signals coming from the short and waveguide *3*, respectively.

Consider, for example, a situation in which a controlled metastructure is given by a waveguide section filled with a metamaterial, as shown in Fig. 1c. In this case, the metastructure can also be represented as a transmission-type Fabry–Perot resonator. Its amplitude reflection and transmission coefficients can be expressed in terms of the length L_{MS} of the metastructure, the propagation constant k_{MS} of the filled waveguide, and the reflection ($r_{mn}^{(A,B)}$) and transmission ($t_{mn}^{(A,B)}$) coefficients measured at the boundaries *A* and *B* between the corresponding waveguide sections:

$$r_{33}^{(MS)} = r_{33}^{(A)} + t_{(fw)3}^{(A)} r_{(fw)(fw)}^{(B)} t_{3(fw)}^{(A)} \times\left[\exp\left(2ik_{MS}L_{MS}\right) - r_{(fw)(fw)}^{(A)} r_{(fw)(fw)}^{(B)}\right]^{-1} \quad (3a)$$

$$r_{CC}^{(MS)} = r_{CC}^{(B)} + t_{C(fw)}^{(B)} r_{(fw)(fw)}^{(A)} t_{(fw)C}^{(B)} \times\left[\exp\left(2ik_{MS}L_{MS}\right) - r_{(fw)(fw)}^{(B)} r_{(fw)(fw)}^{(A)}\right]^{-1} \quad (3b)$$

$$t_{C3}^{(MS)} = t_{(fw)3}^{(A)} t_{C(fw)}^{(B)} \exp\left(-ik_{MS}L_{MS}\right) \times\left[1 - r_{(fw)(fw)}^{(A)} r_{(fw)(fw)}^{(B)} \exp\left(-2ik_{MS}L_{MS}\right)\right]^{-1} \quad (3c)$$

$$t_{3C}^{(MS)} = t_{(fw)C}^{(B)} t_{3(fw)}^{(A)} \exp\left(-ik_{MS}L_{MS}\right) \times\left[1 - r_{(fw)(fw)}^{(B)} r_{(fw)(fw)}^{(A)} \exp\left(-2ik_{MS}L_{MS}\right)\right]^{-1} \quad (3d)$$

The index *(fw)* refers to the filled waveguide section. Formulas (1)–(3) show that the variations of the elements of the ***s***-matrix, the propagation constant k_{MS}, and the coefficients $r_{mn}^{(A,B)}$ and $t_{mn}^{(A,B)}$ defining $r_{mn}^{(MS)}$ and $t_{mn}^{(MS)}$ and, hence, $r^{(FP)}$ due to the external action affect the frequency dependence of the power transmission coefficient from the input to the output $S_{OI}(\omega) = |s|^2 \exp\left[-2\,\mathrm{Im}\left(k_1L_1 + k_2L_2\right)\right]$ and can be viewed in experiments as a control of the interferogram. It is also obvious that the resulting spectrum is much richer than the individual spectra of the tee-interferometer and the Fabry–Perot resonator.

2. Measurement results

The properties of the interferometer are attributed to the spectral characteristics of the metastructure and the superposition of transmitted and reflected, as well as multiply reflected, waves in the Fabry–Perot resonator and the metastructure. To study the functionalities of the interferometer, we consider the effect of different metastructures having different resonance properties and different possibilities of control.

2.1.1. Wire metastructure

Wire metastructure represents a small-period grating cut out from a 0.25-mm-thick commercial material of parallel copper wires (width is 0.1 mm, the distance between the wires is 0.2 mm) embedded into a dielectric film, combined with an orthogonal asymmetrically placed copper strip with a gap loaded with a varactor diodes (Fig. 2a,b,c). The strip is placed on a substrate and is isolated from the grating. A similar metastructure consisting of linear wires in combination with a ferrite plate was earlier considered in [11].

The microwave properties of the metastructure in a waveguide are related to three resonances [27]. One of them (I) is the dipole resonance in the wires of the grating (for a wire length of $\lambda/2$) excited by a microwave electric field E. Another resonance (II) is associated with the excitation of inductive antiparallel currents in U-shaped LC-circuits with capacitive coupling, formed by a pair of adjacent wires of the grating and the corresponding section of the copper strip, that are excited by a microwave magnetic field h directed perpendicular to the plane of the grating. In this case, the total resonance current flows along the wire strip due to the contributions of identically directed currents in each circuit, which determines the third resonance response III in the frequency–amplitude dependence of T. Different types of resonances can be excited separately in given wavelength ranges by appropriately choosing the sizes of the wires and the strip. The resonance III can be shifted by applying a reverse bias voltage V_{DC} to the varactor diode inserted into the gap. The dimensions of the structure are chosen so that, in the frequency band 3–6 GHz of the panoramic VSWR meter, a controlled resonance III is excited in the copper strip, while the resonances I and II are excited at higher frequencies outside this frequency band and do not increase the losses in the interferometer. The resonance III can easily be identified by varying the strip length. To remove spurious resonances due to the induced dc currents, we connect resistors R_L = 100 kΩ to the outputs of the varactor diodes.

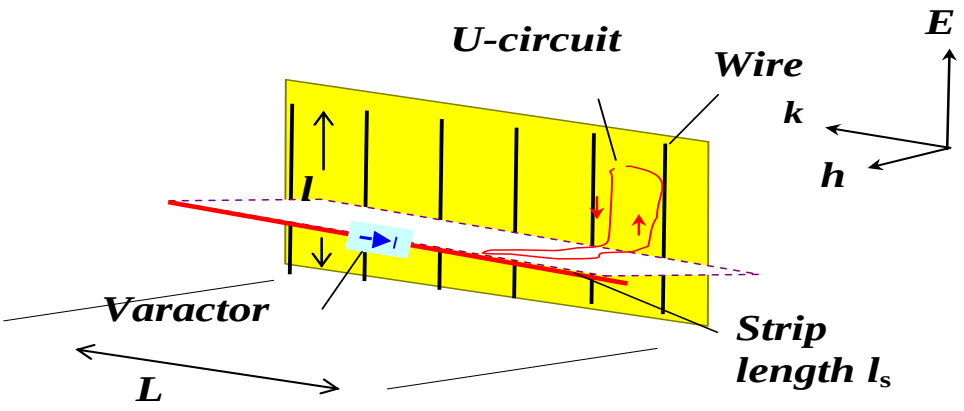

a

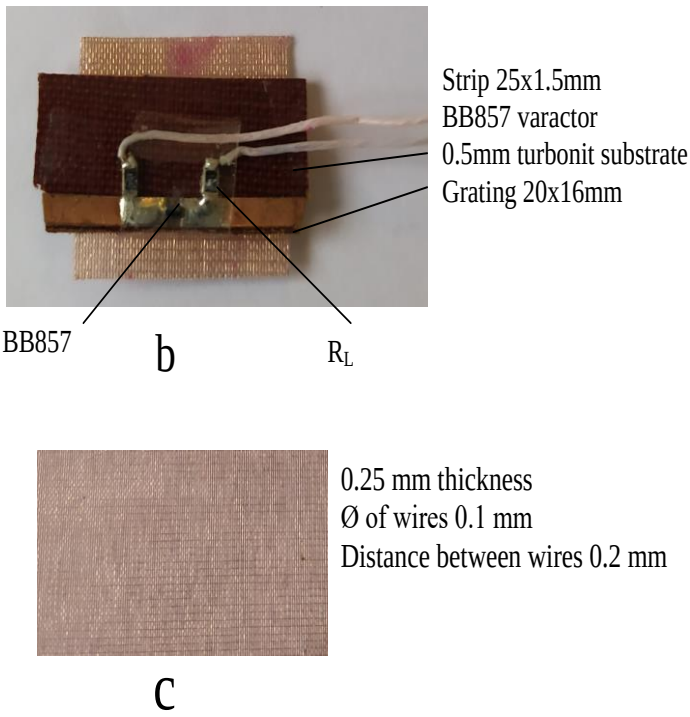

Fig.2. Wire metastructure. (a) Scheme, (b) Photo, (c) Grating material (photo)

The metastructure is presented in Fig 2b (photo). The strip (25x1.5 mm) is placed on 0.5 mm turbonit substrate close by grating (20x16 mm). We use a BB857 varactor diode whose capacitance ranges from 6.5 pF to 0.55 pF under the variation of the reverse bias voltage V_{DC} from 0 to 29 V.

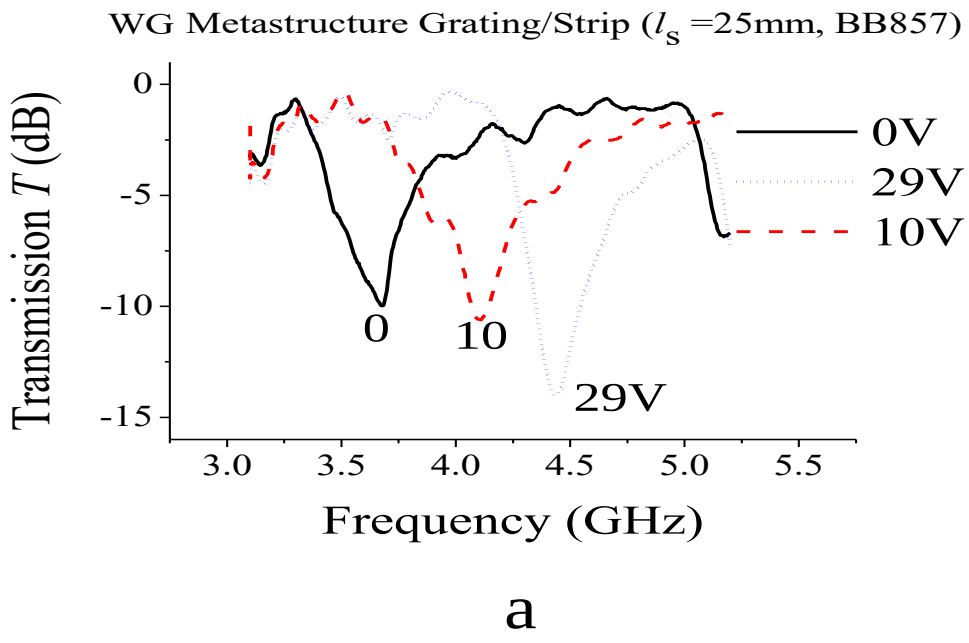

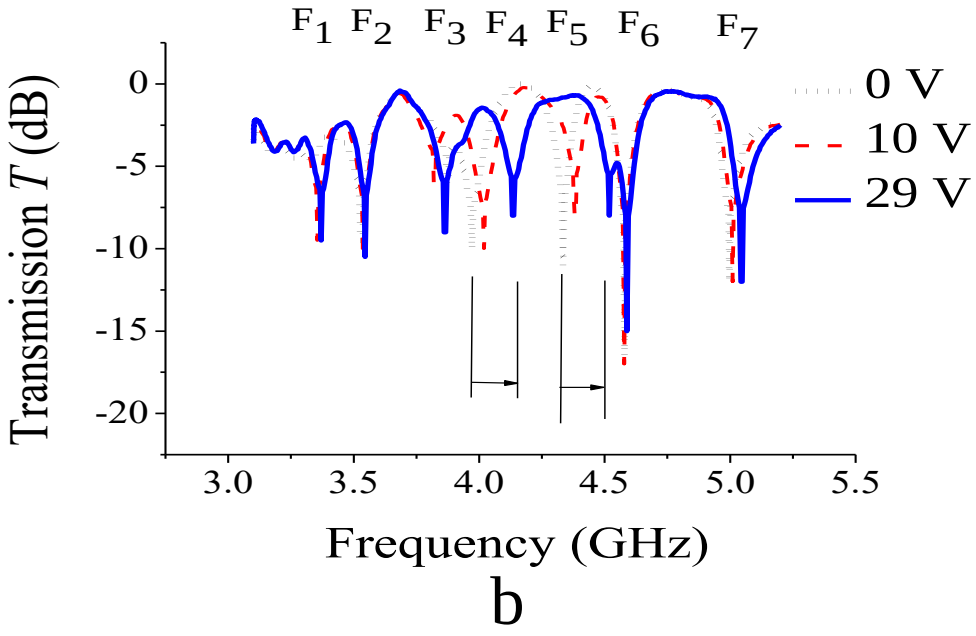

b

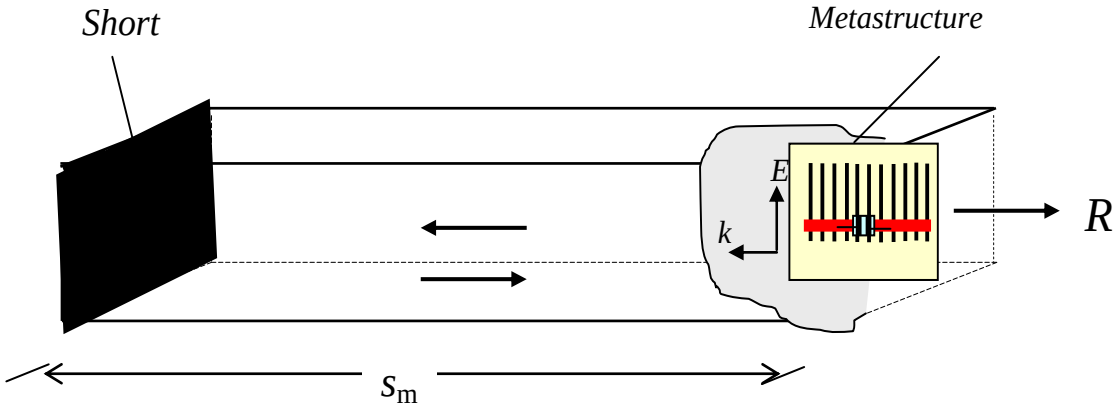

c

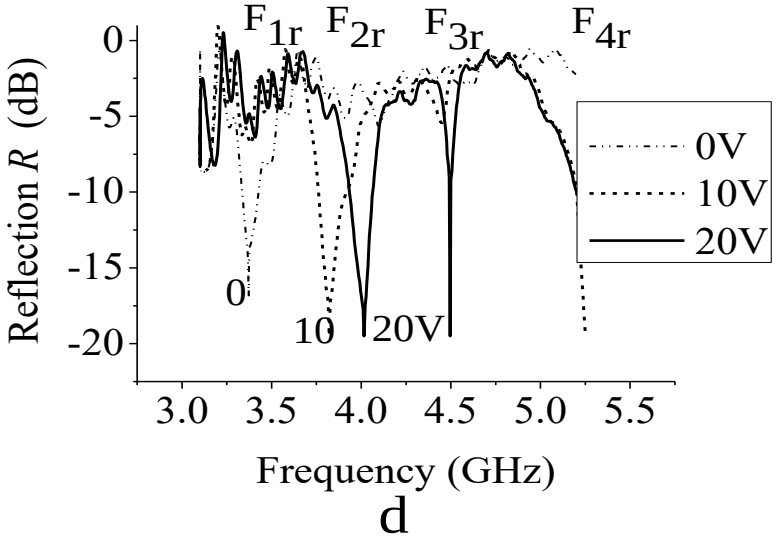

d

Fig. 3. Wire metastructure with BB857 varactor
(a) Transmission *T* (dB) in WG, (b) *T* (dB) in interferometer, (c) scheme of Fabry–Perot resonator, (d) Reflection *R* (dB) from F–P resonator.

The dynamics of the controlled resonance III of the metastructure in the WG is illustrated in Fig. 3a. Under the variation of the reverse bias voltage V_{DC} across the varactor diode from 0 to 29 V, the resonance III in a copper strip is slowly shifted by 0.76 GHz from 3.68 to 4.44 GHz.

Figure 3b demonstrates the measured transmission T versus frequency at the output of the interferometer (Port 2) with metastructure. In the presence of the metastructure, the transmission loses periodicity, an additional stop-band appears, and the interferogram represents an interference dependence of T on frequency with stop-bands F_1^{0V} (frequency f_1^{0V}= 3.37 GHz, depth $T_{1\min}^{0V}$ = –4.6 dB), F_2^{0V} (3.54 GHz, –9.5 dB), F_3^{0V} (3.87 GHz, –6 dB), F_4^{0V} (3.97 GHz, –10 dB) , F_5^{0V} (4.33 GHz, –11 dB), F_6^{0V} (4.58 GHz, –16.5 dB), and F_7^{0V} (5.01 GHz, –12 dB). The application of voltage V_{DC} provides selective electrical control of the bands F_4 and F_5: a shift of frequency with a small variation in the depth ($T_{\min}$). For V_{DC} = 29 V, the band F_4^{29V} is shifted by 0.16 GHz (f_4^{29V} = 4.13 GHz, depth $T_{4\min}^{29V}$= –8 dB), the band F_5^{29V} is shifted by 0.19 GHz (f_5^{29V} = 4.52 GHz, $T_{5\min}^{29V}$= –8 dB). The bands F_1^{29V} (3.37 GHz, –9.5 dB), F_2^{29V} (3.54 GHz, –10.5 dB), F_3^{29V} (3.86 GHz, –9 dB), F_6^{29V} (4.58 GHz, –15 dB), and F_7^{29V} (–5.04 GHz, –12 dB) actually keep their position. In this case, pass-bands are observed instead of the stop-bands F_4^{0V} and F_5^{0V}. The tuning range of interference stop-bands (of about 0.2 GHz) is much narrower than that of the resonance III (0.8 GHz). One can assume that the tuning of the bands is mainly associated with the tuning of the Fabry–Perot resonator, whose frequency is determined not only by its geometric dimensions but also by the resonance properties of the metastructure. To find out this, we perform direct measurements of the controlled characteristics of the resonator (Figs. 3c and 3d), which are of independent interest.

The resonator (Fig. 3c) represents a waveguide section connected to the main waveguide transmission line of the panoramic network analyzer. The waveguide section is short-circuited at one end, and the other end is loaded with a metastructure placed along the waveguide axis at a distance of s = 110 mm from the short. We measure the reflection coefficient R as a function of frequency for different bias

voltages V_{DC} across the varactor diode.

The frequency dependence of R (Fig. 3d) represents a multiband electrically controlled resonance spectrum with bands F_{1r}, F_{2r}, and F_{3r} (the band F_{4r} is shown only partially). For V_{DC} = 0, the band F_{1r} (with frequency f_{1r}^{0V} = 3.37 GHz and a depth of R_{1rmin}^{0V} = –17 dB) is observed, while the bands F_{2r}, F_{3r}, and F_{4r} have a small depth and are poorly displayed.

As the voltage increases to V_{DC} = 10 V, the depth of the band F_{1r} decreases significantly without variation of the frequency (R_{1rmin}^{0V} = –5 dB, f_{1r}^{10V} = 3.37 GHz), the band F_{2r} becomes deeper (R_{2rmin}^{10V} = –19.5 dB, f_{2r}^{10V} = 3.82 GHz), and the band F_{3r} is clearly displayed (R_{3rmin}^{10V} = –5.5 dB, f_{3r}^{10V} = 4.44 GHz). For V_{DC} = 29 V, the band F_{1r} remains unchanged, the band F_{2r} shifts by 0.19 GHz without variation of the depth (f_{2r}^{29V} = 4.01 GHz, $R_{min,\,2r}^{29V}$ = –19.5 dB), and the band F_{3r} becomes deeper and is hardly shifted (R_{3rmin}^{29V} = –19.5 dB, f_{3r}^{29V} = 4.49 GHz).

We can see that, depending on the value of V_{DC}, both the resonance properties of the metastructure (Fig. 3a) and the characteristics of the resonator in the corresponding frequency band are changed. The effect manifests itself when the frequency of resonance III of the metastructure approaches the frequency of the resonance band of the resonator. The band F_{2r} experiences the greatest effect as the resonance III passes through the given frequency range. In this case, the depth and the frequency of the band F_{2r} are changed, and the tunable range and the frequency F_{2r} of the resonator correspond to the tunable range and the frequencies of controlled bands F_4 and F_5 of the interferometer (see Fig. 3b). As a result, the resonant properties of the metastructure affect the interferogram of the interferometer. A wire metastructure is easily implemented and hardly introduces any dielectric losses into the interferogram because the resonances I and II (in the grating and the *LC* circuit) lie outside the frequency range considered. The controlled (and simultaneously controlling) resonance III in the longitudinal strip is excited by a magnetic microwave field *h*, and currents in the strip are not induced by the field *E*. We suppose that the observed losses are primarily due to the varactor diode and the substrate. Let us consider the effect of using a different varactor diode.

2.1.2. MA46H120 varactor loaded strip

The metastructure is presented in Fig. 4a (photo).

The results of investigations with an MA46H120 varactor diode, whose capacitance ranges from 1.15 pF to 0.1 pF under the variation of the reverse bias voltage V_{DC} from 0 to 20 V, are demonstrated in Fig. 4b, c. In this case, the required length of the copper strip is 30 mm to observe a resonance in the frequency range considered. The strip is situated on a 1-mm-thick textolite substrate. The dynamics of the controlled resonance III with the metastructure in a WG is illustrated in Fig. 4b, which demonstrates the measured transmission T and reflection R coefficients as a function of frequency.

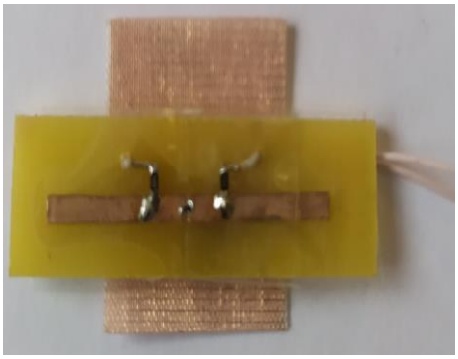

strip 30x1.5mm
MA46H120 varactor
1mm textolite substrate
grating 20x16mm

a

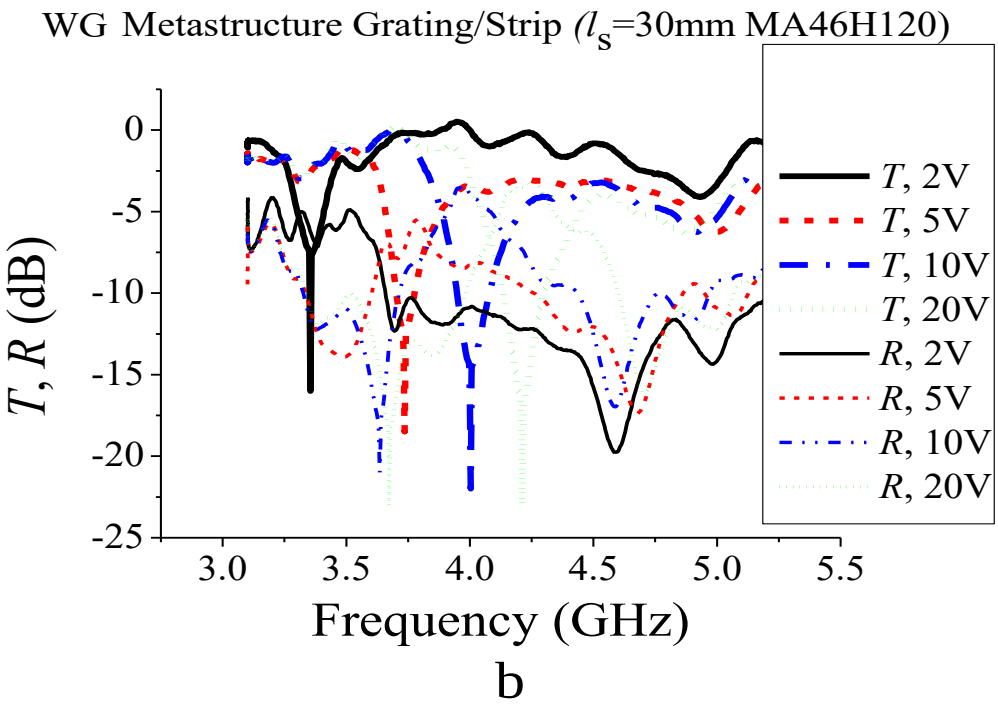

b

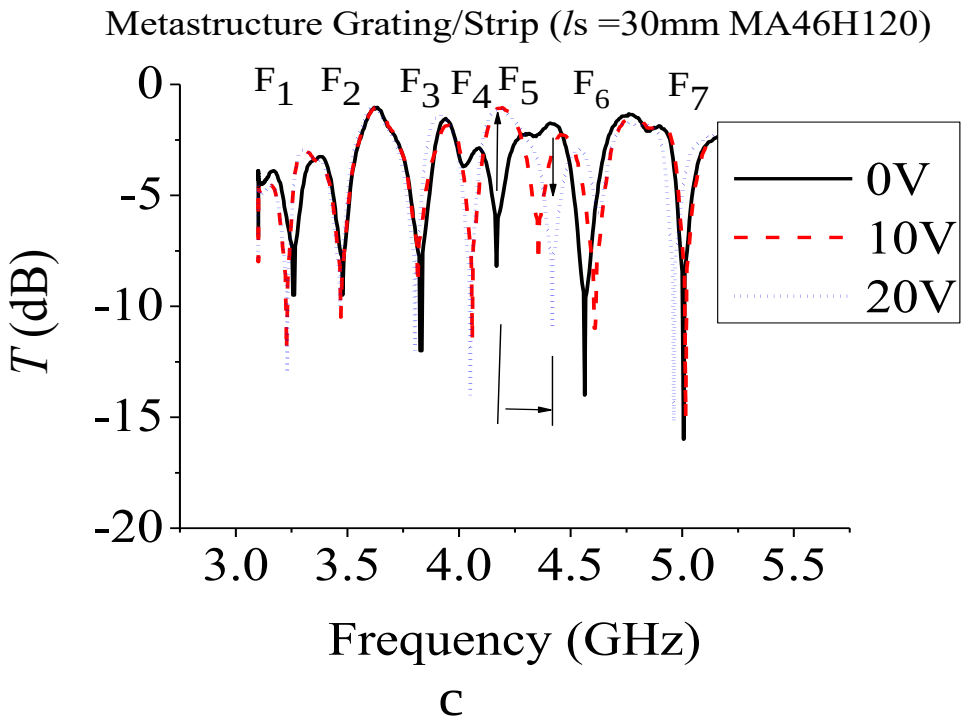

Fig. 4 Wire metastructure with varactor MA46H120
(a) Photo, (b) T (dB) and R (dB) in WG, (c) T (dB) in interferometer.

Under the variation of the reverse bias voltage V_{DC} across the varactor diode from 0 to 20 V, the resonance III in the copper strip is slowly shifted by 0.9 GHz from 3.3 GHz (T_{min}^{0V} = –16 dB, and the corresponding R_{max}^{0V} is about –5 dB) to 4.2 GHz (T_{min}^{20V} = –23 dB, and the corresponding R_{max}^{20V} is about –0.5 dB). Note that, along with a rather broad reflection peak, one can observe a narrow minimum (R_{min} is about –22 dB) at lower frequencies, which is characteristic of magnetic excitation of a resonance. Figure 4b shows that, in the case of an MA46H120 diode, small values of V_{DC} equal to 1 or 2 V already allow tuning of the resonance frequency. Notice also a slight decrease in the insertion loss.

Figure 4c demonstrates the measured transmission T versus frequency at the output of the interferometer (Port 2) with this metastructure. In the presence of the metastructure, the transmission loses periodicity, and the interferogram represents an interference dependence of T on frequency with stop-bands F_1^{0V} (frequency f_1^{0V}= 3.26 GHz, depth T_{1min}^{0V} = –9.5 dB), F_2^{0V} (3.47 GHz, –9.5 dB), F_3^{0V} (3.82 GHz, –12 dB), F_4^{0V} (4.02 GHz, – 3.7 dB) has a small depth, F_5^{0V} (4.16 GHz, –8.2 dB), F_6^{0V} (4.6

GHz, –14 dB), and F_7^{0V} (5 GHz, –16 dB). The application of a voltage of V_{DC} = 10 and 20 V leads to selective tuning of the interferogram in the frequency interval 4–4.5 GHz, which corresponds to the excitation region of the strip. At V_{DC} = 10 V, the interferogram represents the interference dependence of T on frequency with stop-bands F_1^{10V} (frequency f_1^{10V}= 3.23 GHz, depth T_{1min}^{10V} = –=12 dB), F_2^{10V} (3.47 GHz, –10.5 dB), F_3^{10V} (3.81 GHz, –9 dB), F_4^{10V} (4.06 GHz, – 11.5 dB, F_5^{10V} (4.36 GHz, –8 dB), F_6^{10V} (4.6 GHz, –11 dB), and F_7^{10V} (5 GHz, –15 dB). We can see that the stop-band F_5^{10V} shifts by 0.2 GHz relative to F_5^{0V}. In this case, T_{min} in the band F_4^{10V} is changed, and a –0.5 dB pass-band appears in place of the band F_5^{0V}. An increase in V_{DC} to 20 V slightly changes the state of the bands F_4^{20V} (4.05 GHz, –14 dB) and F_5^{20V} (4.42 GHz, –11 dB). We can see that the application of the MA46H120 varactor leads to a slight decrease in the insertion loss and enhances the possibility of tuning at lower values of V_{DC}, without qualitatively changing the dynamics of selective tuning of the interferogram, where a shift of interference band is observed such that a pass-band appears in place of the original stop-band.

2.1.3.Different lengths of strip

Now, we consider whether the method of tuning the resonance frequency in the strip affects the functionalities of the interferometer. To this end, we use a few metastructures with different lengths of the strip (Fig. 5a, photo).

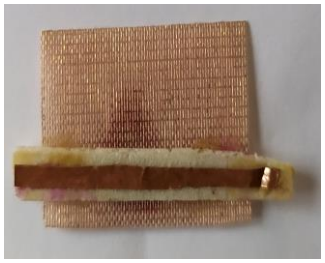

a

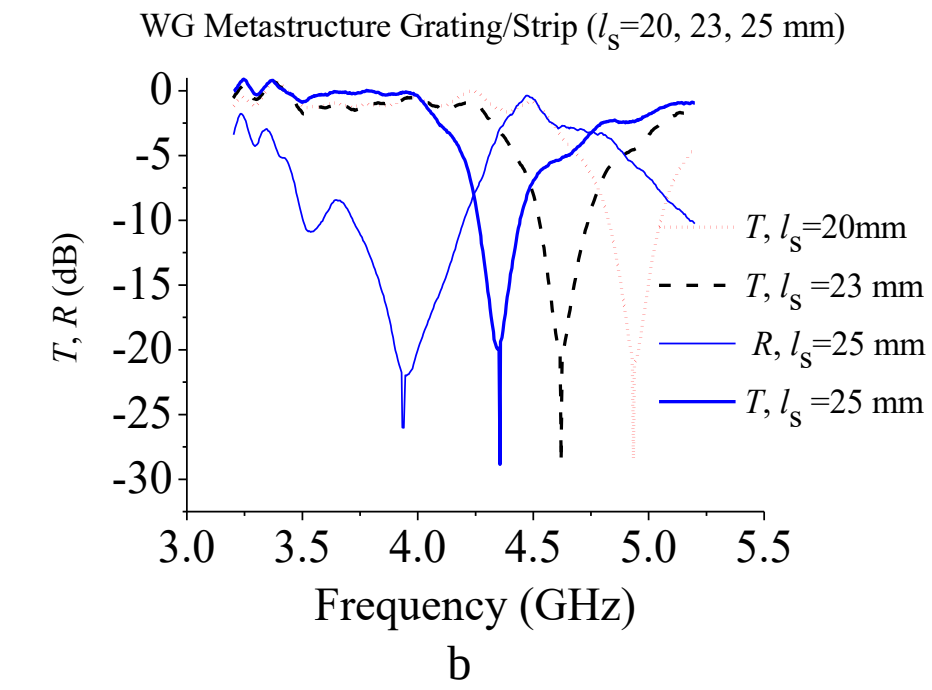

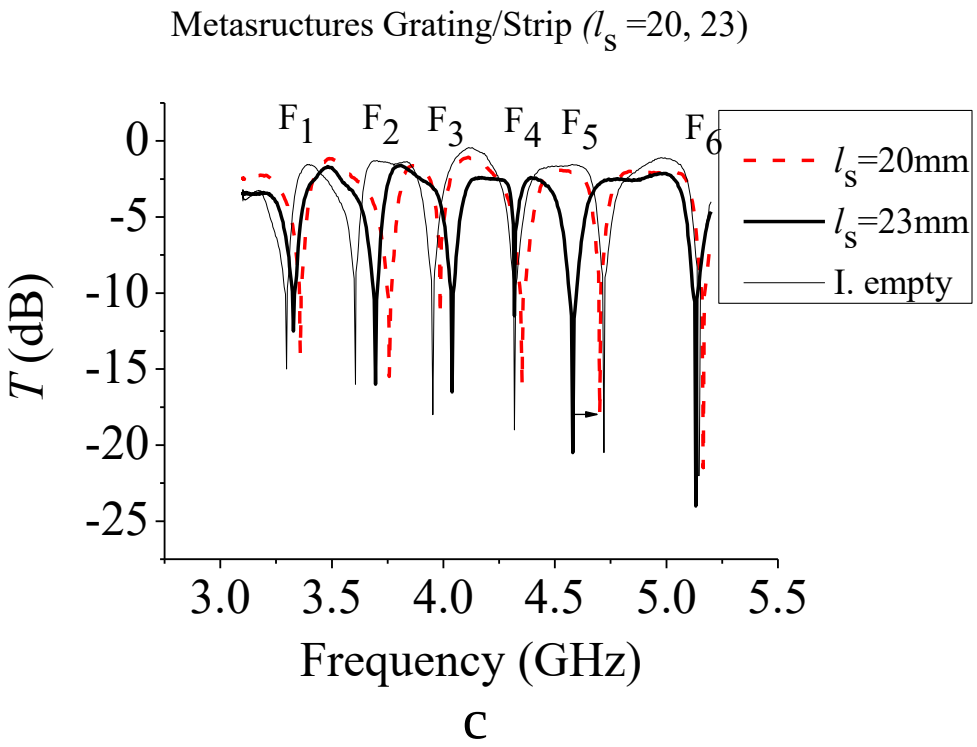

Fig. 5 Wire metastructure, different l_s of strip
(a) Photo, (b) T and R in WG, l_s= 25, 23, 20mm, (c) T (dB) in interferometer, l_s=23, 20mm

This allows us to observe resonances at different frequencies in metastructures without varactor diodes. The results of investigations of metastructures in which a copper strip is deposited on a 1-mm-thick foam substrate orthogonally and asymmetrically with respect to the wires of the grating are shown in Fig. 5b,c. The length l_s of the strip is varied: l_s = 25, 23, and 20 mm.

Figure 5b demonstrates the frequency dependence of the transmission *T* and reflection *R* in the presence of metastructures in a rectangular waveguide. We can see that, for l_s = 25 mm, a resonance is observed at frequency of 4.4 GHz (T_{min} = –28 dB) and shifts by 0.6 GHz for l_s = 20 mm, keeping the value of the insertion loss. The reflection coefficient *R* is characterized by a maximum R_{max} at the frequency of T_{min} and a resonance minimum R_{min} below the frequency of R_{max}. In the case of l_s = 25 mm, R_{min} (–25 dB) is observed at a frequency of 3.9 GHz, while R_{max}, at a frequency of 4.5 GHz.

The frequency dependence of *T* in the interferometer for l_s = 23 and 20 mm, which is illustrated in Fig. 5c, slightly changes the insertion loss of the empty interferometer, in contrast to metastructures with a varactor diode. The interferogram represents an interference dependence of *T* on frequency with stop-bands $F_1^{ls=23}$ (3.3 GHz, –12.5 dB), $F_2^{ls=23}$ (3.7 GHz, –16 dB), $F_3^{ls=23}$ (4 GHz, –16.5 dB), $F_4^{ls=23}$ (4.3 GHz, –11.5 dB), $F_5^{ls=23}$ (4.6 GHz, –20.5 dB), and $F_6^{ls=23}$ (5.1 GHz, –24 dB). For l_s = 20 mm, the interferogram represents an interference dependence of *T* on frequency with stop-bands $F_1^{ls=20}$ (3.4 GHz, –14 dB), $F_2^{ls=20}$ (3.75 GHz, –15.5 dB), $F_3^{ls=20}$ (3.99 GHz, –11.5 dB), $F_4^{ls=20}$ (4.3 GHz, –16 dB), $F_5^{ls=20}$ (4.7 GHz, –18 dB), and $F_6^{ls=20}$ (5.16 GHz, –21.5 dB). We can see that the band $F_5^{ls=20}$ has shifted by 0.1 GHz with respect to $F_5^{ls=23}$ from 4.6 GHz to 4.7 GHz with a small variation in the depth. At the same frequencies, the frequency of resonance III in the metastructure is tuned with an appropriate variation of ls, as it follows from the waveguide measurements (see Fig. 5b). Thus, whatever the method by which the resonance III in the metastructure is tuned (either through the variation of V_{DC} when varactor diodes of various types are used, or through the variation of the strip length), its tuning leads to a selective effect on the stop-band.

2.2. Butterfly dipole

The second metastructure is a (22 x 10 mm) butterfly dipole made from 0.15-mm-thick copper-foiled polyamide film.

2.2.1 MA46H120 loaded butterfly dipole

Butterfly dipole loaded with an MA46H120 varactor diode and excited by a microwave electric field *E* is deposited on a 1-mm-thick textolite substrate (photo 1 in Fig. 6a).

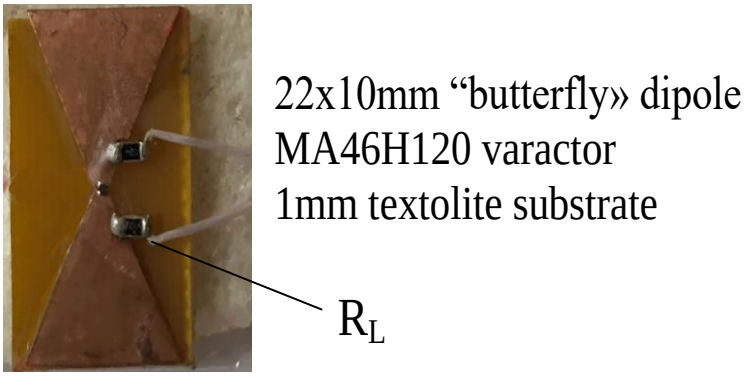

a

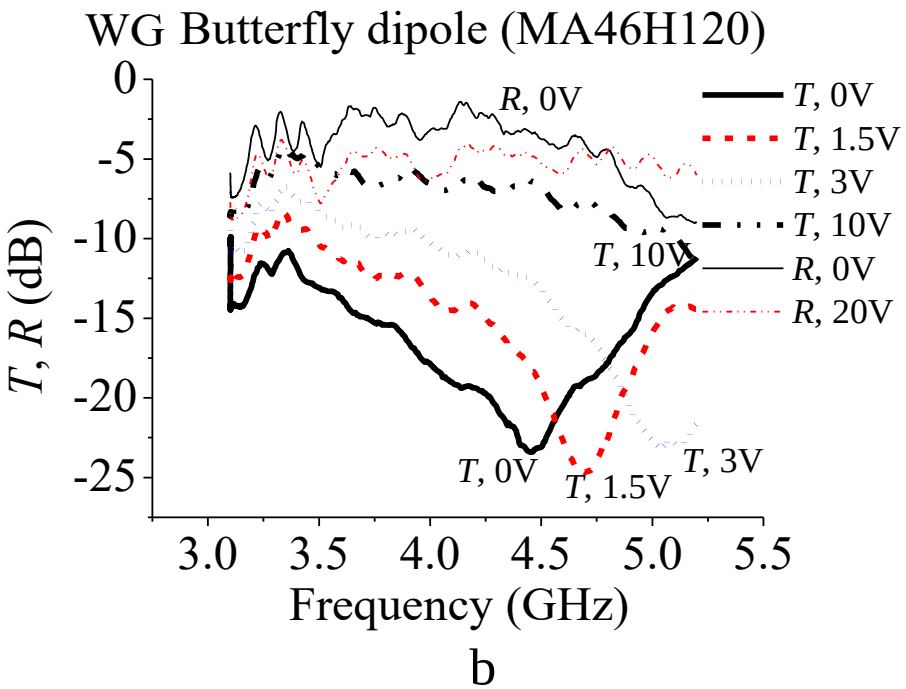

b

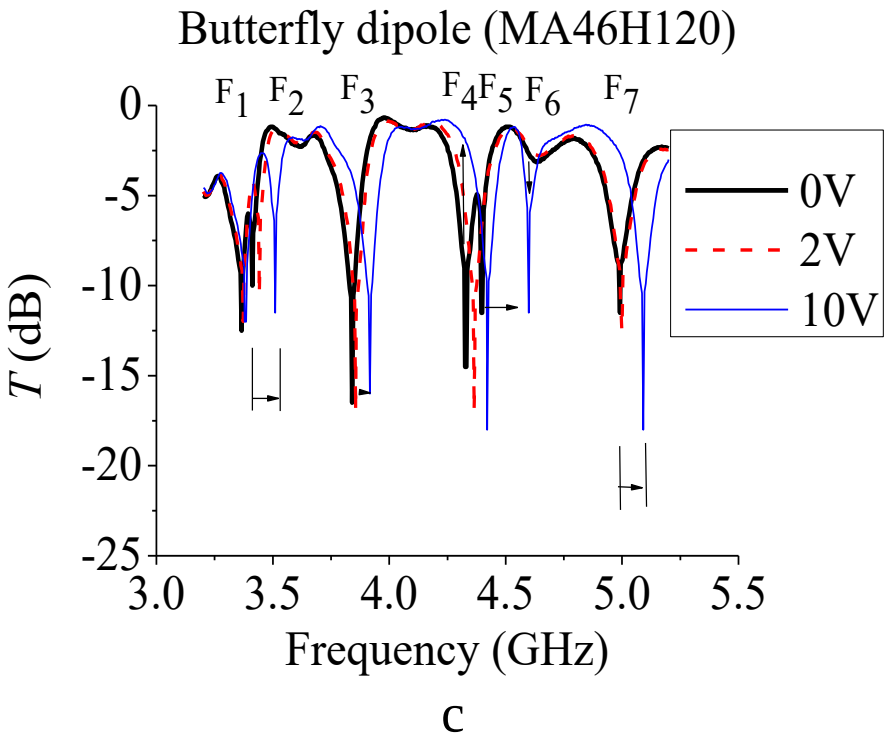

Fig. 6 Butterfly dipole with varactor
(a) Photo, (b) T (dB) and R (dB) in WG, (c) T (dB) in interferometer

Figure 6b demonstrates the frequency dependence of transmission T and reflection R in a WG with a dipole for different values of the reverse bias voltage V_{DC}. We can see a resonance minimum (–23 dB) on the transmission curve T and the corresponding resonance maximum of R (–1.5 dB) related to the broad dipole resonance DR, which slowly shifts by 0.7 GHz from 4.4 to 5.1 GHz under the variation of V_{DC} from 0 to 3 V. The resonance covers almost the entire range considered. Figure 6c demonstrates how the DR affects the state of the interferogram when the dipole is placed along the axis of the shorted h-arm. At zero voltage, V_{DC} = 0, the interferogram represents the interference dependence of T on frequency with stop-bands F_1^{0V} (frequency f_1^{0V}= 3.4 GHz, depth T_{1min}^{0V} = –12.5 dB), F_2^{0V} (3.4 GHz, –10 dB), F_3^{0V} (3.84 GHz, –16.5 dB), F_4^{0V} (4.32 GHz, –14.5 dB), F_5^{0V} (4.4 GHz, –11.5 dB), and F_6^{0V} (5 GHz, –11.5 dB). At V_{DC} = 10 V, the interferogram has the following form: F_1^{10V} (frequency f_1^{10V}= 3.4 GHz, depth T_{1min}^{10V} = –12 dB), F_2^{10V}(3.5 GHz, –11.5 dB), F_3^{10V} (3.9 GHz, –16 dB), F_4^{10V} (4.4 GHz, –18 dB), F_5^{10V} (4.6 GHz,

–11.5 dB), F_6^{10V} (4.6 GHz, –3 dB), F_7^{10V} (5.1 GHz, –18 dB).

We can see that the use of a butterfly dipole enables a specific control of the interferograms (the frequencies and widths of different bands are changed synchronously but not identically). This is associated with the fact that DR is characterized by a rather broad band and its influence covers several interference bands, different bands experiencing different effect of DR.

3.2.2.Fixed capacitance loaded butterfly

Let us consider the control of an interferogram with the use of several dipoles in which, instead of a varactor diode, fixed capacitances of 0.8, 0.5, and 0.1 pF corresponding to the varactor capacitances under the bias voltage V_{DC} are connected to the gaps. Butterfly dipoles are deposited on a 0.5-mm-thick turbonit substrate (Fig. 7a, photo).

22x10mm butterfly dipole
fixed capacitances
0.5mm turbonit substrate

a

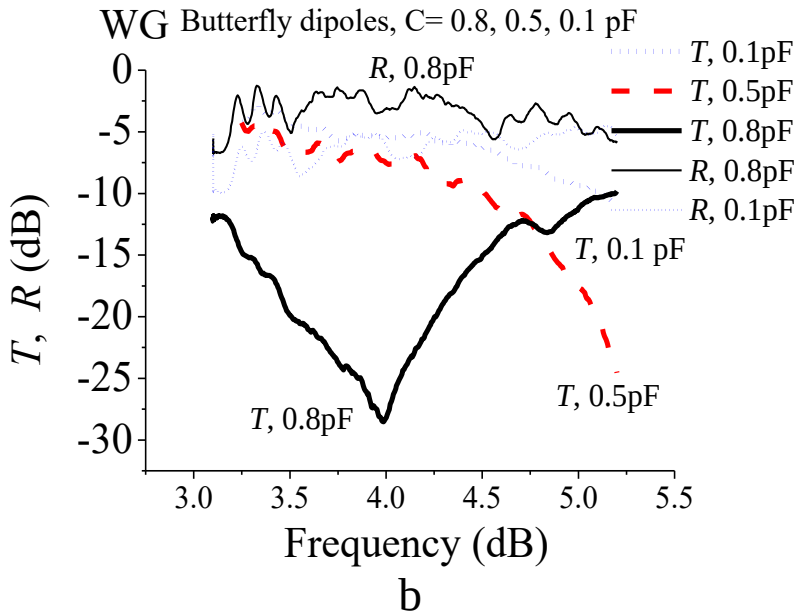

b

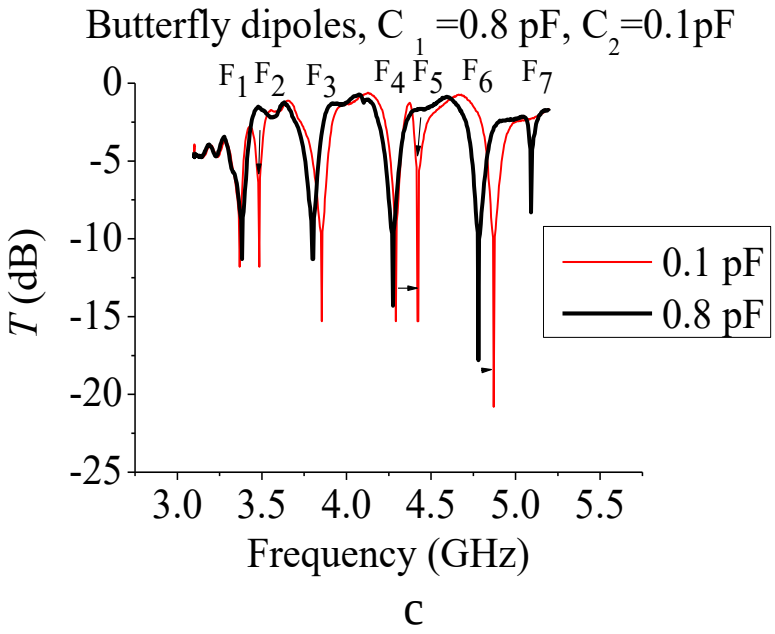

Fig.7 Butterfly dipole with fixed capacitances C
(a) Photo, (b) T (dB) and R (dB) in WG, C = 0.8, 0.5 and 0.1 pF, (c) T (dB) in interferometer, C= 0.8, 0.1 pF

3.3. A row of split ring resonators with varactors MA46H120

Single doubly split ring resonators (with a diameter of 6.6 mm) are deposited by the photolithography technique on a foiled polyamide film. Two MA46H120 varactor diodes are connected to each ring. A row of three rings deposited on a 1-mm-thick textolite substrate (photo in Fig. 8a) is placed along the axis of the shorted *h*-arm of the interferometer at a distance of s_m = 110 mm. The resonance in the rings is excited by a microwave magnetic field directed along the axis of a ring. The resonance dynamics under the voltage V_{DC} is analyzed in a WG, just as in the case of a dipole or a two-layer metastructure when measuring the frequency dependence of the transmission *T* and reflection *R* (Fig. 8b). The resonance that appears as a transmission minimum (–13 dB) and the corresponding reflection maximum (R_{max}^{10V}= –7 dB, R_{max}^{20V} = – 6 dB) slowly shifts to higher frequencies as V_{DC} increases. As V_{DC} changes from 7 to 15 V, the resonance shifts by 0.88 GHz from 3.82 GHz to 4.7 GHz, while keeping the insertion loss.

The dynamics of the interferogram of the interferometer under the variation of V_{DC} is illustrated in Fig. 8c. At zero V_{DC}, the interferogram represents an interference

dependence of T on frequency with stop-bands F_1^{0V} (frequency f_1^{0V}= 3.35 GHz, depth $T_{1\min}^{0V}$ = –9.3 dB), F_2^{0V} (3.6 GHz, –7.3 dB), F_3^{0V} (3.95 GHz, –9.8 dB), F_4^{0V} (4.38 GHz, –12 dB) , F_5^{0V} (4.71 GHz, –13 dB), and F_6^{0V} (5.14 GHz, –19.3 dB). At V_{DC} = 5.5 V, the band $F_2^{5.5V}$ is affected, and the interferogram has the form: $F_1^{5.5V}$ (frequency $f_1^{5.5V}$= 3.33 GHz, depth $T_{1\min}^{5.5V}$ = –9.3 dB), $F_2^{5.5V}$ (3.59 GHz, –5.4 dB), $F_3^{5.5V}$ (3.97 GHz, –10.3 dB), $F_4^{5.5V}$ (4.4 GHz, –12.3 dB) , $F_5^{5.5V}$ (4.73 GHz, –13 dB), and $F_6^{5.5V}$ (5.17 GHz, –20.3 dB). The next band F_3 is affected at V_{DC} = 7.5 V; to change the shape and the width of the band F_4, we should apply V_{DC} = 10.5. V; the band F_5 is affected at V_{DC} = 12.5 V. In these cases, the interferograms have the form:

$F_1^{7.5V}$ (frequency $f_1^{7.5V}$= 3.33 GHz, depth $T_{1\min}^{7.5V}$ = –9.8 dB), $F_2^{7.5V}$ (3.58 GHz, –8.3 dB), $F_3^{7.5V}$ (3.9 GHz, –6.5 dB), $F_4^{7.5V}$ (4.36 GHz, –11.8 dB) , $F_5^{7.5V}$ (4.68 GHz, –13 dB), and $F_6^{7.5V}$ (5.1 GHz, –20.3 dB);

$F_1^{10.5V}$ (frequency $f_1^{10.5V}$= 3.35 GHz, depth $T_{1\min}^{10.5V}$ = –11 dB), $F_2^{10.5V}$ (3.6 GHz, –9.5 dB), $F_3^{10.5V}$ (3.95 GHz, –11.5 dB), $F_4^{10.5V}$ (4.4 GHz, –5 dB) , $F_5^{10.5V}$ (4.74 GHz, –15 dB), and $F_6^{10.5V}$ (5.16 GHz, –21.5 dB); $F_1^{12.5V}$ (frequency $f_1^{12.5V}$= 3.35 GHz, depth $T_{1\min}^{12.5V}$ = –11.5 dB), $F_2^{12.5V}$ (3.59 GHz, –10.5 dB), $F_3^{12.5V}$ (3.93 GHz, –12 dB), $F_4^{12.5V}$ (4.32 GHz, –13 dB) , $F_5^{12.5V}$ (4.7 GHz, –5.5 dB)**,** and $F_6^{12.5V}$ (5.1 GHz, –22 dB); We can see that, as V_{DC} changes, $T_{\min}$ increases and simultaneously increases the bandwith together with the variation of its shape; in this case, one may observe bifurcated resonances. We assume that these phenomena are associated with coupled resonances in the rings and interference bands as their resonance frequencies approach each other. Thus, ring resonators in the interferometer allow the electrical control of each band by turns, since a rather narrow resonance is excited in the rings. The application of V_{DC} may change the shape and width of an individual stop-band almost without changing the spectrum of other bands (Fig. 8c).

The observed effect may also manifest itself in the case of a combination of split ring resonators with other metastructures or elements.

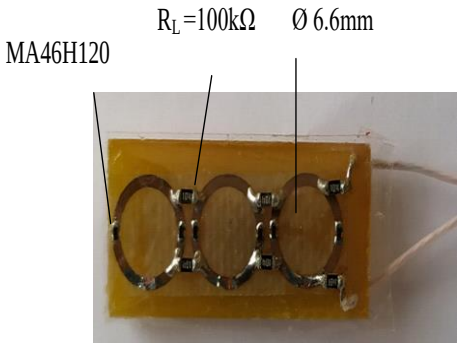

a

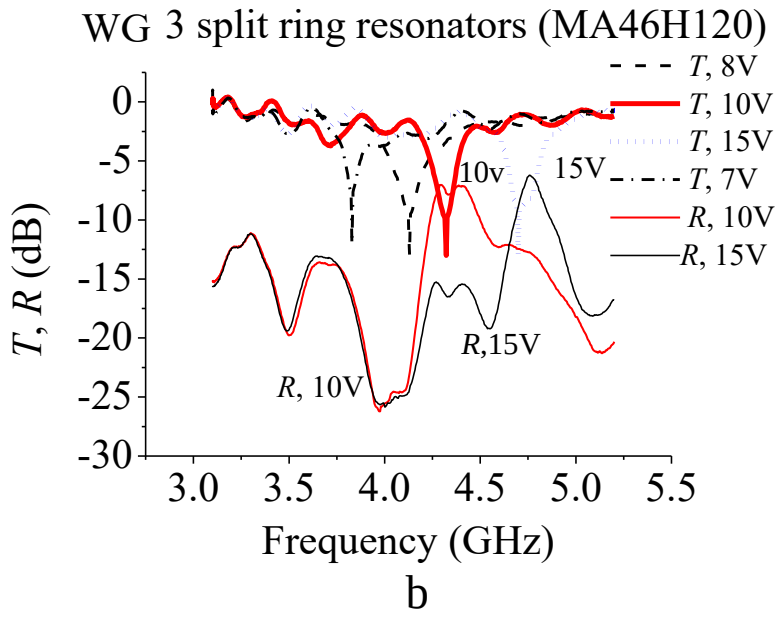

b

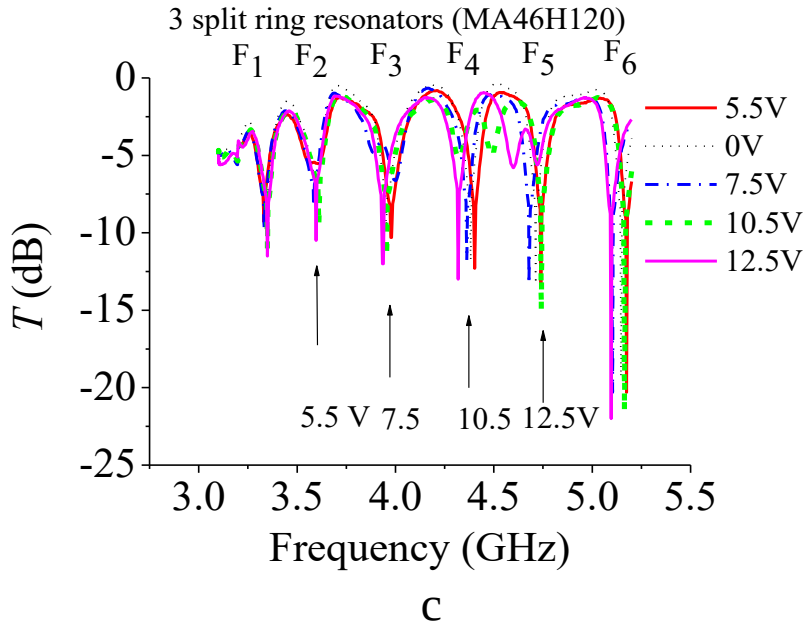

c

Fig. 8 Row of split ring resonators
(a) Photo, (b) T (dB) and R (dB) in WG, (c) T (dB) in interferometer.

Conclusions

In this work we have investigated for the first time a modified 3–6-GHz-band waveguide tee interferometer that contains a metastructure with a varactor diode and forms, together with a short, a controlled Fabry–Perot resonator. We have revealed that the resonance in the metastructure selectively affects a stop-band of the interferometer. We have demonstrated the possibility to form and efficiently transform various selectively electrically tunable functionalities of interferometer through the use of various varactor-loaded metastructures.

We have demonstrated selective tuning of the band center frequency (within 0.2 GHz with a wire metastructure and a butterfly dipole), or a selective change in the shape and width of each stop-band by turns (with split ring resonators), or a change in the shape and width of each stop-band and the center frequency independently (with a sandwich of split ring resonators/butterfly dipole.

A distinctive feature of the proposed interferometer is that it allows one to design a variety of multiband filters by choosing an appropriate metastructure, by varying the distance s_m between the metastructure and the short, and by varying the bias voltage. The results obtained can be useful for the design of multifunctional multichannel communication systems.

Acknowledgments

The work was carried out within the framework of the state task 0030-2019-0014.

References

1. Cameron R.J., Kudsia C.M., Mansour R.R. *Microwave Filters for Communication Systems: Fundamentals, Design, and Applications*. JohnWiley & Sons. Inc. 2018. 928 p.
2. Entesari K., Rebeiz G.M. A 12-18-GHz three-pole RF MEMS tunable filter. *IEEE Trans. Microw. Theory Techn.*, 2005. Vol.53. No.8. P.2566-2571.
3. Huang F., Fouladi S., Mansour R. High-Q tunable dielectric resonator filters using MEMS technology. *IEEE Trans. Microw. Theory Techn.* 2011. Vol.59**.** No.12. P.3401-3409. Part 2, SI.

4. Kozhevnikov A.V., Khivintsev Yu.V., Dudko, G.M. et al. Filtration of Surface Magnetostatic Waves in Yttrium Iron Garnet Films of Variable Width Excited by Focusing Transducers. *Technical Physics Letters*. 2018. Vol.44. No.8. P.705–708.
5. Bi K., Zhu W., Lei M et al. Magnetically tunable wideband microwave filter using ferrite-based metamaterials. *Appl. Phys. Lett*. 2015. Vol.106. No.17. P.173507.
6. Sharma D., Khare N., Koul S.K. et al. Spur-line based magnetically tunable bandstop filter using partially magnetized ferrite thin films. *Appl. Phys. Lett*. 2017. Vol.110. No.18. P.182401.
7. Jiang H., Lacroix B., Choi K. et al. Ka- and U-band tunable bandpass filters using ferroelectric capacitors. *IEEE Trans. Microw. Theory Techn.* 2011. Vol.59. No.12. P.3068-3075, Part 1.
8. Mias C. Waveguide and free-space demonstration of tunable frequency selective surface. *Electron. Lett.* 2003, Vol.39. No.11. P.850 – 852.
9. Jung M., Min B-W. A Widely Tunable Compact Bandpass Filter Based on a Switched Varactor-Tuned Resonator. *IEEE Access*,. 2019. No.**7**. P.95178-95185.
10. Butylkin V., Kazantsev Y., Kraftmakher G. et al. Voltage-controlled unidirectional propagation of microwaves in metastructures ferrite/conductive elements with varactors. *Appl. Phys. A.* 2017. Vol.123. No.1. P.57 .
11. Kraftmakher G., Butylkin V., Kazantsev Y. et al. Microwave tunable and switchable planar non-reciprocal three-layer multiresonant wire–ferrite metastructure. *Electron. Lett.* 2017. Vol.53. No.18. P.1264–1266.
12. Krupka J., Cwikla A., Mrozowski M. et al. High Q-factor microwave Fabry-Perot resonator with distributed Bragg reflectors. *IEEE Transactions on Ultrasonics, Ferroelectrics and Frequency Control.* 2005. Vol.52. No.9. P.1443–1451.
13. Liu Z.G., Zhang W.X. Fu D.L. et al. Broadband Fabry-Perot resonator printed antennas using FSS superstrate with dissimilar size. *Microwave and Optical Technology Letters*. 2008. Vol.50. No.6. P.1623 – 1627.

14. Liu B., Wei F., Shi X. Reconfigurable bandpass filter based on net-type stepped-impedance resonator. *Electron. Lett.* 2010. Vol.46. No.22. P.1506-1507.
15. Kaur T., Osorio L., Olvera-Cervantes J.L. et al. Microfluidic Reconfigurable Filter Based on Ring Resonators. *Progress In Electromagnetics Research Letters.* 2018. Vol.79. P.59 – 63.
16. Gómez-García R., Guyette A.C. Reconfigurable Multi-Band Microwave Filters. *IEEE Trans. Microw. Theory Techn.* 2015. Vol.63. No.4. P.1294 – 1307.
17. Kumar M.S., Choukiker Y.K. Tunable wideband frequency and switching polarization reconfiguration antenna for wireless applications. *IET Microwaves, Antennas & Propagation.* 2018. Vol.12**.** No.15. P.2364 – 2371.
18. Chen F.-C., Li R.-S., Chen J.-P. A Tunable Dual-Band Bandpass-to-Bandstop Filter Using p-i-n Diodes and Varactors. *IEEE Access.* 2018. No.6. P.46058 – 46065.
19. Zhang Y-J., Cai J., Chen J-X. Design of Novel Reconfigurable Filter With Simultaneously Tunable and Switchable Passband. *IEEE Access*. 2019. No.7. P.59708-59715.
20. Yang T., Rebeiz G.M. Bandpass-to-bandstop reconfigurable tunable filters with frequency and bandwidth controls. *IEEE Trans. Microw. Theory Techn.* 2017. Vol.65. No.7. P.2288-2297.
21. Al-Yasir Y.I.A., Parchin N.O., Abd-Alhameed R.A. et al. Resent Progress in the Design of 4G/5G Reconfigurable Filters. *Electronics.* 2019. Vol.8. P.114–131.
22. Xiao-Ping Chen, Ke Wu. Substrate Integrated Waveguide Filters: Design Techniques and Structure Innovations. *IEEE Microwave Magazine*, September. 2014. Vol.15. P.121-133.
23. Varikuntla K.K., Singaravelu R. Design of SIW cavity models to control the bandwidth of frequency selective surface. *IET Microwave Antennas & Propagation.* 2019. Vol.13. No.14. P.2515-2524.
24. Fok M.P., Ge J. Tunable Multiband Microwave Photonic Filters. *Photonics.* 2017. Vol.4. No.4. P.45.

25. Ustinova I.A., Nikitin A.A., Kondrashov A.V. et al. A microwave interferometer based on a ferrite–ferroelectric layered structure. *Tech. Phys. Lett*. 2016. Vol.42. No.9. P.891–894.
26. Kraftmakher G.A., Butylkin V.S., Kazantsev Yu.N. et al. Magnetically and Electrically Controlled Microwave Interference Pattern in a Meta-Interferometer. *JETP Letters*. 2019. Vol.109. No.4. P.232-238.
27. Kraftmakher G., Butylkin V. Cut wires grating – single longitudinal wire' planar metastructure to achieve microwave magnetic resonance in a single wire. *Advanced Electromagnetics*. 2012. Vol.1.No.2. P.16 -25.
28. Stone J.M. *Radiation and Optics: An Introduction to the Classical Theory*. New York, McGraw-Hill. 1963. 544 p.

For citation:
Kraftmakher G.A., Butylkin V.S., Kazantsev Yu.N., Mal'tsev V.P., Nikitin I.P. A tunable multiband microwave filter based on a waveguide tee interferometer containing Fabry–Perot resonator with a metastructure as a reflector. *Zhurnal Radioelektroniki - Journal of Radio Electronics*. 2020. No. 6. https://doi.org/10.30898/1684-1719.2020.6.15